

Aggregation Schemes for Single-Vector WSI Representation Learning in Digital Pathology

Sobhan Hemati, Ghazal Alabtah, Saghir Alfasly, H.R. Tizhoosh

KIMIA Lab, Department of Artificial Intelligence and Informatics,
Mayo Clinic, Rochester, MN, USA

Abstract. A crucial step to efficiently integrate Whole Slide Images (WSIs) in computational pathology is assigning a single high-quality feature vector, i.e., one embedding, to each WSI. With the existence of many pre-trained deep neural networks and the emergence of foundation models, extracting embeddings for sub-images (i.e., tiles or patches) is straightforward. However, for WSIs, given their high resolution and gigapixel nature, inputting them into existing GPUs as a single image is not feasible. As a result, WSIs are usually split into many patches. Feeding each patch to a pre-trained model, each WSI can then be represented by a set of patches, hence, a set of embeddings. Hence, in such a setup, WSI representation learning reduces to set representation learning where for each WSI we have access to a set of patch embeddings. To obtain a single embedding from a set of patch embeddings for each WSI, multiple set-based learning schemes have been proposed in the literature. In this paper, we evaluate the WSI search performance of multiple recently developed aggregation techniques (mainly set representation learning techniques) including simple average or max pooling operations, Deep Sets, Memory networks, Focal attention, Gaussian Mixture Model (GMM) Fisher Vector, and deep sparse and binary Fisher Vector on four different primary sites including bladder, breast, kidney, and Colon from TCGA. Further, we benchmark the search performance of these methods against the median of minimum distances of patch embeddings, a non-aggregating approach used for WSI retrieval.

Keywords: Histopathology · Whole Slide Image · WSI · Image Representation · WSI Search · Set Representation Learning · Single-Vector · Aggregation

1 Introduction

The image analysis field has witnessed remarkable advancements in recent years, thanks to the integration of deep learning models and the availability of large-scale data. However, analysis of histopathology images using deep learning is not as straightforward as ordinary-sized images. Especially, to build whole slide image (WSI) search engines, the most critical step is to be able to measure the similarity between WSIs efficiently and accurately [1,2]. The state-of-the-art approach to this step is to extract high-quality deep embeddings that capture tissue

morphology from each WSI using a well-trained deep model. To this end, it is necessary to feed WSIs to build such models. However, given the gigapixel nature of WSIs, feeding a WSI at high magnification into a model to GPU memory is infeasible. To overcome this challenge, a WSI is usually split into a set of much smaller sub-images called “patches” or tiles. Following this procedure, we end up with a set of deep embeddings per WSI which makes it challenging to employ them for downstream tasks like WSI retrieval (a set of patches that could be very large if a smart patch selection is not available). In this situation, having one single-vector WSI embedding can mitigate such challenges. With single-vector WSI representation much less memory is required to build a WSI search system. As well, using distance measures calculating similarity between WSIs becomes trivial. Finally, the search speed will increase and storage requirements will decrease resulting in wider deployment of WSI image classification and retrieval.

A practical and established approach to calculate the similarity between two sets of embeddings is the *median-of-minimums*, a scheme that was introduced as part of the Yottixel search engine [3]; one calculates the minimum distance of any given input patch to all other patches (of the other WSI) and takes the median of all minimum distances overall (see Fig. 1). This approach is quite practical and fast (as Yottixel used binary feature vectors) but it is not able to provide a single vector to represent WSI. A more desirable solution would be to obtain *one single embedding* per WSI for more efficient storage and more targeted WSI-to-WSI matching, or for WSI classification (Fig. 2).

To this end, different aggregation algorithms to derive a single vector of deep features from a set of patch embeddings have been proposed including simple average or max pooling operations, Deep Sets [4], memory networks [5], focal attention [6], graph convolution neural networks [7], Gaussian mixture model (GMM) Fisher Vector [8,9,10], and Deep Fisher Vector and its variations (binary and sparse Fisher Vector) [10].

Although multiple set representation learning techniques have been proposed and investigated in the literature, to the best of our knowledge, there is no study that evaluates these algorithms against each other for WSI retrieval as a challenging task. To address this shortcoming, in this paper, we briefly introduce each set representation learning technique and discuss our benchmarking scheme. Subsequently, we evaluate each method over four different datasets namely bladder, breast, kidney, and colon through the k -Nearest Neighbour (k -NN) search using WSI embeddings obtained from each method. Finally, in the result section we present and discuss the performance of each technique to generate a single vector of deep features for a WSI.

1.1 Statement of Significance

Whole Slide Image (WSI) representation learning is a cornerstone of computational pathology, enabling efficient retrieval, classification, and analysis of gigapixel-scale histopathology images. However, the challenge lies in deriving a single high-quality feature vector for an entire WSI, given that existing GPUs

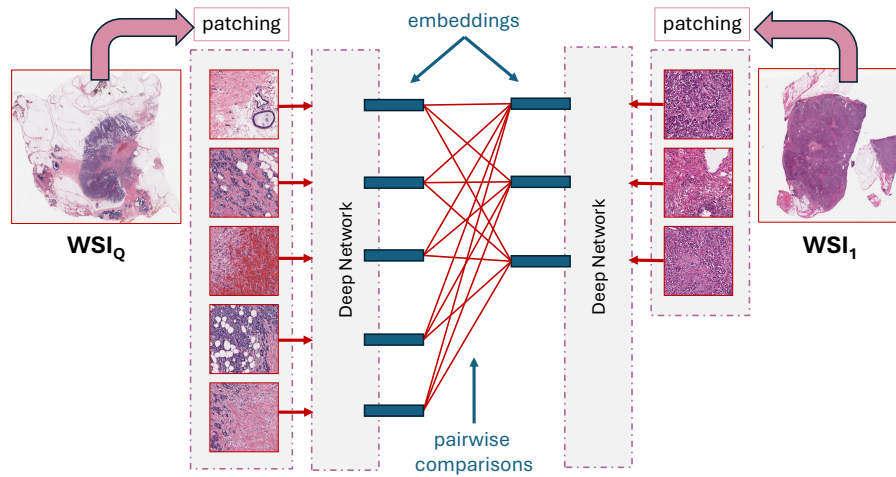


Fig. 1: Yottixel [3], although a patch-oriented search engine, introduced the first practical approach for WSI-to-WSI comparison through the median-of-minimum distance measurements.

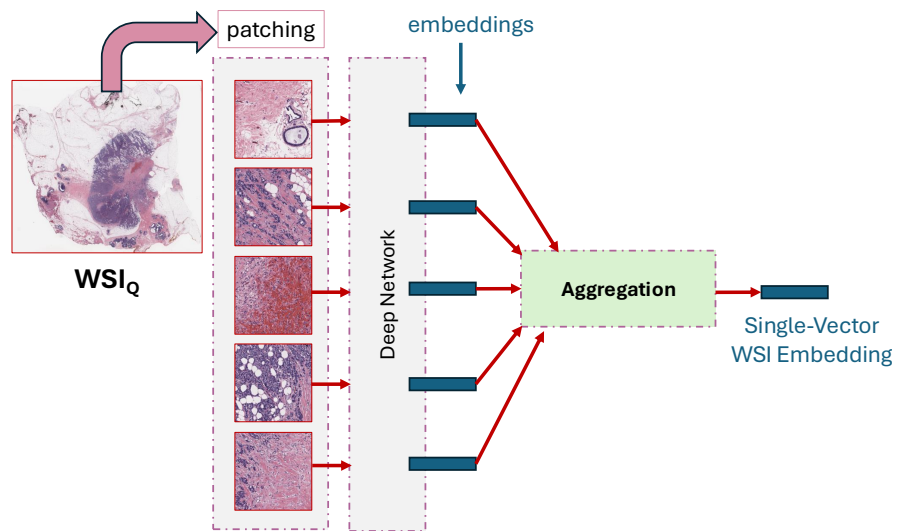


Fig. 2: Aggregation of patch embeddings can provide a single-vector WSI representation.

cannot process them as single images due to their enormous resolution. Traditionally, WSIs are divided into smaller patches, each independently embedded using deep neural networks, leading to a set-based representation problem where optimal aggregation strategies remain an open question. This study systematically evaluates multiple state-of-the-art set representation learning techniques—including Deep Sets, Memory Networks, Focal Attention, Gaussian Mixture Model (GMM) Fisher Vector, and deep sparse and binary Fisher Vector—against conventional pooling methods for WSI embedding aggregation. Additionally, we benchmark these approaches against a non-aggregating retrieval technique based on the median of minimum distances of patch embeddings. Our comprehensive evaluation, conducted on TCGA datasets across four cancer types (bladder, breast, kidney, and colon), provides critical insights into the effectiveness of different aggregation strategies for WSI search and retrieval. By rigorously comparing various WSI embedding aggregation techniques, this study advances the field of computational pathology by guiding researchers and practitioners toward more effective and computationally feasible WSI retrieval methodologies. The findings have significant implications for large-scale histopathology archives, image-based precision medicine, and AI-driven diagnostic workflows.

2 Background

In this section, we briefly review set representation learning algorithms applied to the WSI representation learning problem.

2.1 GMM Fisher Vector (1999-2007)

Fisher Vector can be seen as an extension to bag of visual words (BoVW) [11] that was initially developed in computer vision research for encoding a set of local image descriptors into one embedding. Theoretically, Fisher Vector can be developed on top of any generative models [8]. Some works [9] have introduced Gaussian mixture model (GMM)-based Fisher Vector which can be calculated using the gradient of the log-likelihood of the GMMs with respect to its parameters given a bag of data points (e.g., means, variances, and mixing coefficients). Theoretically, while BoVW only employs mean statistics to obtain the set representation, in the GMM-based Fisher Vector, the variance as a higher-order statistic is also used.

2.2 Deep Sets (2017-2021)

The Deep Set approach [4] focuses on permutation invariant representation learning and establishes a standard definition of the permutation invariant functions. This approach shows such a family of functions can be implemented as neural networks to learn permutation invariant representations. Other works employ

Deep Sets-like architecture along with CNN to learn end-to-end WSI representations in WSI search tasks [12]. These methods showed the obtained representations achieve better search performance both in terms of search speed and accuracy compared with Yottixel search engine [3].

2.3 Memory Networks (2020)

Other works have presented Memory-based Exchangeable Model (MEM) to learn the permutation invariant set functions [5]. In this method, a MEM is constructed from multiple memory blocks where each memory block is a sequence-to-sequence model containing multiple memory units. The output of each memory block is invariant to the permutations of the input sequence. The memory units are in charge of calculation of attention values for each instance. To calculate these attention values, the memory vectors are aggregated using a pooling operation (weighted averaging) to form a permutation-invariant representation. Increasing the number of memory units enables the memory block to capture more complex dependencies between the instances of a set by providing an explicit memory representation for each instance in the sequence. MEM was evaluated on point cloud and lung WSIs classification.

2.4 Focal Attention (2021)

Another set representation scheme developed for WSI classification/search is Focal attention [6]. This approach was inspired by two recent developments in representation learning literature, focal loss and attention based MIL [13] and proposed the novel pooling layer called focal attention (FocAtt-MIL) where all patches of a mosaic are mapped into a single embedding using an attention-weighted averaging [13] modulated by a trainable focal factor. More precisely, FocAtt-MIL is composed from four main components. Prediction MLP, WSI Context, Attention Module, and Focal Network. The Prediction MLP is a trainable neural network that calculates a prediction for each patch embedding in the set. WSI context is also a neural network (basically Deep Sets from [4] that obtains one embedding per WSI in a simple efficient manner that capture general information from the WSI. The attention module is made from two MLPs transformation, and the Attention networks. The attention module takes the patch embedding and WSI context and output the an attention value between 0 to 1 for each instance. Finally, the focal network receive the WSI context and computes a focal factor per dimension which further guides the final prediction toward better WSI representation.

2.5 Deep Fisher Vector and its variations (2023)

Motivated by the success of GMM-based Fisher Vector, Fisher Vector theory has been proposed for more recent deep generative models including Variational Autoencoders (VAEs) [14] and GANs [15]. Recently, other works have extended

VAE-based Fisher Vectors for the WSI representation learning task [10]. More specifically, this approach offered two variations of Deep Fisher Vectors, namely “*deep sparse Fisher Vector*” and “*deep binary Fisher Vector*”, to obtain binary and sparse permutation-invariant WSI embeddings suitable for downstream tasks such as efficient WSI search. To obtain the deep sparse, and binary Fisher Vectors, one can employ a simple VAE where its latent space is also connected to a dense layer with a softmax activation function that outputs a probability distribution representing the predicted WSI class. This classifier injects class information (i.e., diagnosis) into the final WSI embeddings. Considering that the Fisher Vector is derived from the gradient space of the VAE, to achieve sparse or binary embeddings, it is desired to have sparse or minimum quantization loss gradients. This step has been performed with a gradient regularization loss which is calculated using double backpropagation [10]. Finally, the total loss for training the VAE consists of a weighted summation of reconstruction loss, KL divergence loss, classification loss, and gradient regularization loss. The contribution of gradient regularization loss to the total loss is controlled through the α regularization parameter. Fig. 3 shows the training architecture.

After training the VAE, first, the gradients of the reconstruction loss are computed. Second, the gradient using power and L_2 normalization steps are normalized (see [16]). Finally, considering that the dimensionality of the deep Fisher Vector is the same as the number of the VAE parameters (which can be a large number making the WSI search expensive), the effective dimensions are selected to be the top M parameters that provide the highest variance in their respective gradient values for the training data. Fig. 4 shows the calculation of single-vector WSI representation given the trained VAE and patch embeddings for a WSI.

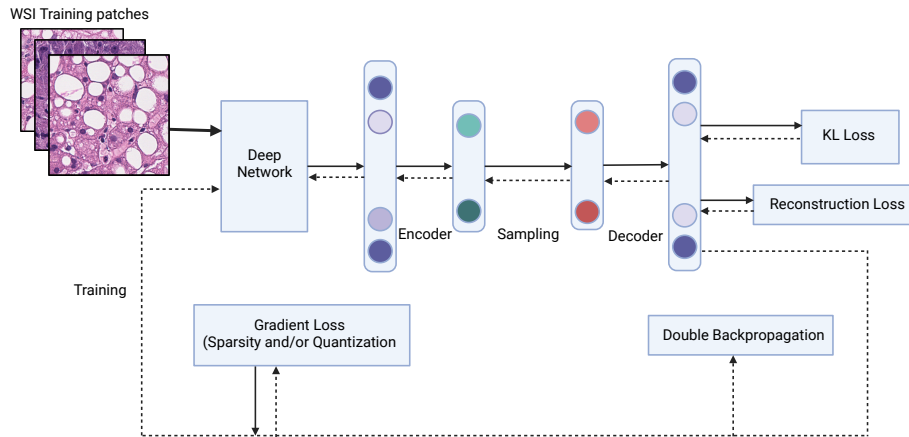


Fig. 3: VAE Training architecture

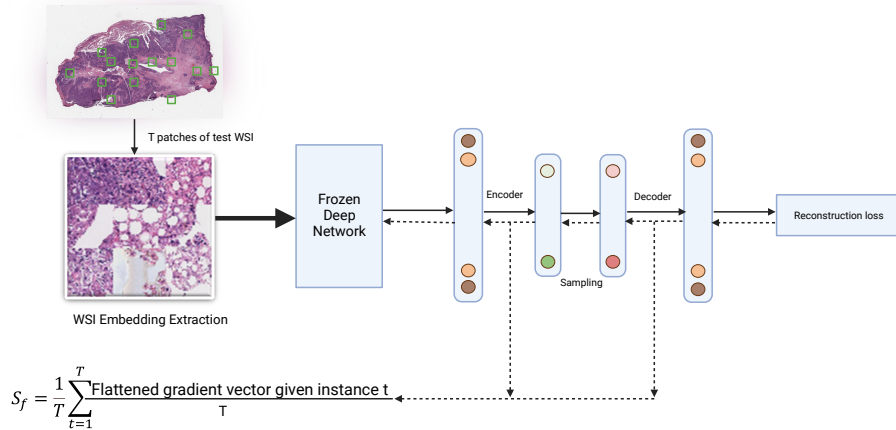


Fig. 4: Aggregation to generate a single-vector WSI embedding.

2.6 Other Approaches

Recently foundation models for multiple WSI representation learning have been proposed that use various techniques for aggregation of patch embedding, including GIGAPATH [17], PRISM [18], CHIEF [19], and THREADS [20]. Among these works, GIGAPATH [17] and THREADS [20] require embeddings for all patches from WSI to perform the aggregation. Given that the backbones are generally foundation models, such techniques are extremely expensive in practice. Additionally, CHIEF [19] and PRISM [18] use techniques based on the attention-based MIL by [13]. Considering that here we already discussed two different extensions of the attention-based MIL namely Focal attention [6] and Memory-based Exchangeable Model [5] techniques, we did not include the aggregation techniques in CHIEF [19] and PRISM.

In terms of acquiring expressive embeddings, foundation models have been reported to be inaccurate for zero-shot WSI retrieval [21], insensitive to inter-center variations [22], and exhibit low rotational invariance [23]. Moreover, they consume approximately 35 times more energy than conventional deep models, are not easily fine-tunable, and still require large amounts of data for downstream tasks [24].

3 Methodology

This paper aims to compare the performance of the multiple set aggregation techniques for WSI representation learning including simple average or max pooling operations, Deep Sets, Memory networks, Focal attention, Gaussian Mixture Model (GMM) Fisher Vector, and deep sparse and binary Fisher Vector. We validate these methods for the task of WSI retrieval. Hence, we must construct

an evaluation framework involving different datasets, and baselines. In this section, first, we discuss the datasets, the benchmarking task and baselines.

3.1 Datasets

The datasets presented in this study contain a collection of four histopathology cases, including bladder, breast, kidney, and colon primary sites disease cases. All datasets are drawn from The Cancer Genome Atlas (TCGA). For each WSI, multiple patches were extracted using Yottixel’s mosaic algorithm (a two-staged clustering approach that employs stain histograms and patch proximity to group patches) [3]. Each patch is represented by an embedding extracted from DenseNet [25] with imageNet pre-trained weights encoding the structural information and unique characteristics of the corresponding histological region.

Bladder Dataset – The skin data contains 457 cases with 6 different subtypes as classes. The subtypes include ‘Transitional cell carcinoma’, ‘Papillary transitional cell carcinoma’, ‘Cholangiocarcinoma’, ‘Squamous cell carcinoma-NOS’, ‘Papillary adenocarcinoma-NOS’, ‘Carcinoma-NOS’.

Breast Dataset – The breast dataset contains 1,133 WSIs, with 23 subtypes including ‘Lobular carcinoma-NOS’, ‘Infiltrating duct carcinoma-NOS’, ‘Infiltrating duct mixed with other types of carcinoma’, ‘Adenoid cystic carcinoma’, ‘Infiltrating duct and lobular carcinoma’, ‘Intraductal micropapillary carcinoma’, ‘Large cell neuroendocrine carcinoma’, ‘Apocrine adenocarcinoma’, ‘Mucinous adenocarcinoma’, ‘Metaplastic carcinoma-NOS’, ‘Infiltrating lobular mixed with other types of carcinoma’, ‘Carcinoma-NOS’, ‘Paget disease and infiltrating duct carcinoma of breast’, ‘Pleomorphic carcinoma’, ‘Papillary carcinoma-NOS’, ‘Phyllodes tumor-malignant’, ‘Secretory carcinoma of breast’, ‘Intraductal papillary adenocarcinoma with invasion’, ‘Cribriform carcinoma-NOS’, ‘Medullary carcinoma-NOS’, ‘Tubular adenocarcinoma’, ‘Basal cell carcinoma-NOS’, ‘Malignant lymphoma-large B-cell-diffuse-NOS’.

Kidney Dataset – the kidney contains 6 subtypes and 940 cases from TCGA. The subtypes include ‘Papillary adenocarcinoma-NOS’, ‘Clear cell adenocarcinoma-NOS’, ‘Renal cell carcinoma-NOS’, ‘Giant cell sarcoma’, ‘Renal cell carcinoma-chromophobe type’, ‘Synovial sarcoma-spindle cell’.

Colon Dataset – The colon dataset has 459 cases from TCGA that contain 9 classes, ‘Adenocarcinoma-NOS’, ‘Mucinous adenocarcinoma’, ‘Adenosquamous carcinoma’, ‘Adenocarcinoma with neuroendocrine differentiation’, ‘Adenocarcinoma with mixed subtypes’, ‘Carcinoma-NOS’, ‘Papillary adenocarcinoma-NOS’, ‘Dedifferentiated liposarcoma’, ‘Malignant lymphoma-large B-cell-diffuse-NOS’.

3.2 Benchmarking Scheme and Baselines

WSI search and retrieval offers many benefits including teleconsultation, reduced workload, improved diagnostic quality, and expedited adoption and democratization of digital pathology through more efficient indexing of tissue images [26,27]. Considering these benefits, we are motivated to investigate the quality of WSI

Experiment	Accuracy	Macro $\bar{F}1$	Weighted $\bar{F}1$
Average Pooling	0.820	0.448	0.789
Deep Binary Fisher Vector	0.852	0.471	0.827
Deep Sets (Max)	0.835	0.473	0.804
Deep Sets (Mean)	0.846	0.513	0.828
Deep Sets (Prod)	0.824	0.470	0.799
Deep Sets (Sum)	0.833	0.427	0.797
Deep Sparse Fisher Vector	0.859	0.525	0.835
Fisher Vector	0.857	0.510	0.830
Focal Attention (Max)	0.818	0.435	0.786
Focal Attention (Mean)	0.800	0.392	0.761
Focal Attention (Sum)	0.831	0.398	0.791
Max Pooling	0.829	0.486	0.810
Memory Network (Max)	0.818	0.413	0.803
Memory Network (Mean)	0.796	0.329	0.768
Memory Network (Prod)	0.802	0.450	0.780
Memory Network (Sum)	0.837	0.362	0.780
Yottixel Median of Minima	0.796	0.375	0.757

Table 1: Bladder Metrics

embeddings through the lens of k -Nearest Neighbors (k -NN) WSI search and retrieval.

The accuracy, Macro F1 score, and weighted F1 score performance measures are used as the evaluation metrics. We benchmark multiple techniques against Yottixel’s “median of minimums” as a non-aggregation approach [3]. We test max and mean poolings, Gaussian Mixture Model-based Fisher Vector [28], Deep Sets [4], memory networks [5], focal attention [6], and deep sparse Fisher Vector and deep binary Fisher Vector by [10].

Except for the median of minimums, all methods lead to a single embedding per WSI. Further, the deep Fisher Vector provides both binary and sparse WSI embeddings which are ideal for fast and efficient WSI search. These representations are memory-efficient, ensuring that the embeddings can be economically stored and efficiently processed for subsequent retrieval and analysis tasks. To ensure the reliability of the results, a rigorous 5-fold cross-validation approach is employed. We compute the average and standard deviation from the five splits and use these as performance indicators.

4 Results

Tables 1, 2, 3 and 4 show the evaluation results for bladder, breast, kidney, and colon datasets where *DenseNet* was used as feature extractors. Clearly, in most cases, Deep Fisher Vector and its variations (sparse and binary) achieve the best overall performance compared with all other baselines. Here we should emphasize sparse embeddings can reduce the memory required to store embeddings

Experiment	Accuracy	Macro $\bar{F}1$	Weighted $\bar{F}1$
Average Pooling	0.667	0.103	0.615
Deep Binary Fisher Vector	0.695	0.125	0.644
Deep Sets (Max)	0.640	0.111	0.613
Deep Sets (Mean)	0.626	0.095	0.604
Deep Sets (Prod)	0.644	0.109	0.611
Deep Sets (Sum)	0.636	0.111	0.613
Deep Sparse Fisher Vector	0.692	0.132	0.647
Fisher Vector	0.692	0.146	0.639
Focal Attention (Max)	0.652	0.086	0.605
Focal Attention (Mean)	0.647	0.085	0.599
Focal Attention (Sum)	0.629	0.073	0.578
Max Pooling	0.640	0.100	0.601
Memory Network (Max)	0.588	0.068	0.545
Memory Network (Mean)	0.622	0.068	0.556
Memory Network (Prod)	0.621	0.067	0.526
Memory Network (Sum)	0.592	0.061	0.472
Yottixel Median of Minima	0.620	0.068	0.564

Table 2: Breast Metrics

while binary WSI embeddings provide both memory efficiency and extremely fast search speed by employing Hamming distance. As a sample case, we also measured the time required to conduct the colon dataset search experiment for both Deep Sparse and Binary Fisher Vectors and also the median of minimums. For the Sparse Fisher Vector, Euclidean distance is used while for the Binary Fisher Vector Hamming distance is employed. The results for this experiment are presented in Table 5. Clearly, the Deep Binary Fisher Vector achieves the fastest search speed. Given that for the Sparse Fisher Vector the Euclidean distance is used, its search speed is the same as other methods that output one real-valued embedding (with the same dimension) per WSI.

4.1 Ablation study

To study the effect of the gradient sparsity and quantization losses for Deep Sparse and Binary Fisher vector embeddings respectively, we performed an ablation study on α for skin and lung datasets. To this end, we train the VAE for different values of α , while keeping all other hyperparameters the same. The results for breast and colon datasets are presented in Tables 6 and 7. Clearly, including the regularization loss further improves the quality of embeddings while increasing memory and speed efficiency by introducing binary nature and sparsity characteristics for WSI embedding.

Experiment	Accuracy	Macro $\bar{F}1$	Weighted $\bar{F}1$
Average Pooling	0.702	0.469	0.681
Deep Binary Fisher Vector	0.802	0.590	0.798
Deep Sets (Max)	0.763	0.549	0.756
Deep Sets (Mean)	0.760	0.549	0.755
Deep Sets (Prod)	0.747	0.535	0.741
Deep Sets (Sum)	0.764	0.547	0.756
Deep Sparse Fisher Vector	0.793	0.586	0.787
Fisher Vector	0.799	0.572	0.788
Focal Attention (Max)	0.534	0.301	0.503
Focal Attention (Mean)	0.568	0.351	0.544
Focal Attention (Sum)	0.555	0.315	0.525
Max Pooling	0.690	0.464	0.669
Memory Network (Max)	0.644	0.364	0.589
Memory Network (Mean)	0.650	0.393	0.628
Memory Network (Prod)	0.639	0.377	0.596
Memory Network (Sum)	0.492	0.163	0.331
Yottixel Median of Minima	0.472	0.248	0.441

Table 3: Kidneys Metrics

5 Conclusion

In this paper, we evaluated multiple WSI representation learning techniques including simple average or max pooling operations, deep sets, memory networks, focal attention, Gaussian Mixture Model (GMM) Fisher Vector, and deep sparse and binary Fisher Vector embeddings in the WSI search task for different datasets and two different deep models. Our evaluations show that the deep sparse and binary Fisher Vector may achieve the best overall performance compared with multiple set aggregation schemes. This result suggests that the Fisher Vector method has a robust ability to capture relevant patterns and features within the data, regardless of the specific characteristics of each dataset. This is an important indication of the versatility and generalizability of the Fisher Vector approach. Apart from their superior WSI search performance, deep sparse and binary Fisher Vectors also offer additional advantages that are suitable for fast and efficient search and retrieval. More precisely, the sparsity in deep sparse Fisher Vector embeddings makes them occupy less storage for indexing WSIs, a crucial factor for the wide adoption and also democratization of digital pathology. Also, the deep binary Fisher Vector is significantly faster than any real-valued counterpart as the calculation of Hamming distance between binary embeddings can be calculated using the XOR gate at the CPU level which is extremely faster than Euclidean distance.

Experiment	Accuracy	Macro $\bar{F}1$	Weighted $\bar{F}1$
Average Pooling	0.807	0.322	0.771
Deep Binary Fisher Vector	0.809	0.302	0.789
Deep Sets (Max)	0.839	0.377	0.795
Deep Sets (Mean)	0.802	0.317	0.779
Deep Sets (Prod)	0.830	0.343	0.785
Deep Sets (Sum)	0.818	0.297	0.782
Deep Sparse Fisher Vector	0.807	0.281	0.776
Fisher Vector	0.825	0.313	0.788
Focal Attention (Max)	0.807	0.332	0.770
Focal Attention (Mean)	0.816	0.322	0.769
Focal Attention (Sum)	0.825	0.327	0.776
Max Pooling	0.825	0.312	0.784
Memory Network (Max)	0.805	0.285	0.758
Memory Network (Mean)	0.798	0.301	0.754
Memory Network (Prod)	0.820	0.291	0.760
Memory Network (Sum)	0.843	0.297	0.773
Yottixel Median of Minima	0.802	0.298	0.757

Table 4: Colon Metrics

Dimensions	Sparse	Binary	Yottixel
30,000	1,659,800 ms	690,026 ms	
3,000	1,491,833 ms	601,359 ms	1,007,515 ms
300	1,815,617 ms	475,188 ms	

Table 5: Time required for different dimensions of Fisher vector for Sparse and Binary methods for the Colon dataset compared to Yottixel

References

1. Hamid R Tizhoosh and Liron Pantanowitz. On image search in histopathology. *Journal of Pathology Informatics*, page 100375, 2024.
2. Isaiah Lahr, Saghir Alfasly, Peyman Nejat, Jibrán Khan, Luke Kottom, Vaishnavi Kumbhar, Areej Alsaafin, Abubakr Shafique, Sobhan Hemati, Ghazal Alabtah, Nneka Comfere, Dennis Murphree, Aaron Mangold, Saba Yasir, Chady Meroueh, Lisa Boardman, Vijay H. Shah, Joaquin J. Garcia, and H.R. Tizhoosh. Analysis and validation of image search engines in histopathology. *IEEE Reviews in Biomedical Engineering*, pages 1–19, 2024.
3. Shivam Kalra, Hamid R Tizhoosh, Charles Choi, Sultaan Shah, Phedias Diamandis, Clinton JV Campbell, and Liron Pantanowitz. Yottixel—an image search engine for large archives of histopathology whole slide images. *Medical Image Analysis*, 65:101757, 2020.
4. Manzil Zaheer, Satwik Kottur, Siamak Ravanbakhsh, Barnabas Poczos, Russ R Salakhutdinov, and Alexander J Smola. Deep sets. *Advances in neural information processing systems*, 30, 2017.
5. Shivam Kalra, Mohammed Adnan, Graham Taylor, and Hamid R Tizhoosh. Learning permutation invariant representations using memory networks. In *Computer*

α	Breast (Sparse)			Breast (Binary)		
	Accuracy	Macro $\bar{F}1$	Weighted $\bar{F}1$	Accuracy	Macro $\bar{F}1$	Weighted $\bar{F}1$
0.0	0.690	0.151	0.651	0.685	0.126	0.640
0.1	0.693	0.149	0.650	0.703	0.131	0.653
0.01	0.698	0.140	0.651	0.697	0.123	0.646
0.001	0.702	0.145	0.660	0.684	0.115	0.636
0.0001	0.688	0.137	0.646	0.691	0.114	0.637
0.00001	0.706	0.144	0.663	0.680	0.116	0.634

Table 6: Results for Sparse and Binary Fisher vector methods for Breast dataset with different values of α , including Accuracy, Macro $\bar{F}1$, and Weighted $\bar{F}1$

α	Colon (Sparse)			Colon (Binary)		
	Accuracy	Macro $\bar{F}1$	Weighted $\bar{F}1$	Accuracy	Macro $\bar{F}1$	Weighted $\bar{F}1$
0.0	0.825	0.358	0.789	0.807	0.274	0.778
0.1	0.820	0.339	0.782	0.807	0.307	0.785
0.01	0.820	0.340	0.782	0.811	0.277	0.783
0.001	0.814	0.330	0.776	0.818	0.288	0.790
0.0001	0.816	0.316	0.778	0.820	0.312	0.786
0.00001	0.816	0.334	0.780	0.805	0.301	0.779

Table 7: Results for Sparse and Binary Fisher vector methods for Colon dataset with different values of α , including Accuracy, Macro $\bar{F}1$, and Weighted $\bar{F}1$

Vision-ECCV 2020: 16th European Conference, Glasgow, UK, August 23–28, 2020, Proceedings, Part XXIX 16, pages 677–693. Springer, 2020.

6. Shivam Kalra, Mohammed Adnan, Sobhan Hemati, Taher Dehkharghanian, Shahryar Rahnamayan, and Hamid R Tizhoosh. Pay attention with focus: A novel learning scheme for classification of whole slide images. In *Medical Image Computing and Computer Assisted Intervention–MICCAI 2021: 24th International Conference, Strasbourg, France, September 27–October 1, 2021, Proceedings, Part VIII 24*, pages 350–359. Springer, 2021.
7. Mohammed Adnan, Shivam Kalra, and Hamid R Tizhoosh. Representation learning of histopathology images using graph neural networks. In *Proceedings of the IEEE/CVF Conference on Computer Vision and Pattern Recognition Workshops*, pages 988–989, 2020.
8. Tommi Jaakkola and David Haussler. Exploiting generative models in discriminative classifiers. In *Advances in neural information processing systems*, pages 487–493, 1999.
9. Florent Perronnin and Christopher Dance. Fisher kernels on visual vocabularies for image categorization. In *2007 IEEE conference on computer vision and pattern recognition*, pages 1–8. IEEE, 2007.
10. Sobhan Hemati, Shivam Kalra, Morteza Babaie, and HR Tizhoosh. Learning binary and sparse permutation-invariant representations for fast and memory efficient whole slide image search. *Computers in Biology and Medicine*, 162:107026, 2023.
11. Gabriella Csurka, Christopher Dance, Lixin Fan, Jutta Willamowski, and Cédric Bray. Visual categorization with bags of keypoints. In *Workshop on statistical*

- learning in computer vision, ECCV*, volume 1, pages 1–2. Prague, 2004.
12. Sobhan Hemati, Shivam Kalra, Cameron Meaney, Morteza Babaie, Ali Ghodsi, and Hamid Tizhoosh. Cnn and deep sets for end-to-end whole slide image representation learning. In *Medical Imaging with Deep Learning*, pages 301–311. PMLR, 2021.
 13. Maximilian Ilse, Jakub Tomczak, and Max Welling. Attention-based deep multiple instance learning. In *International conference on machine learning*, pages 2127–2136. PMLR, 2018.
 14. Zhaofan Qiu, Ting Yao, and Tao Mei. Deep quantization: Encoding convolutional activations with deep generative model. In *Proceedings of the IEEE Conference on Computer Vision and Pattern Recognition*, pages 6759–6768, 2017.
 15. Shuangfei Zhai, Walter Talbott, Carlos Guestrin, and Joshua Susskind. Adversarial fisher vectors for unsupervised representation learning. *Advances in Neural Information Processing Systems*, 32, 2019.
 16. Florent Perronnin, Jorge Sánchez, and Thomas Mensink. Improving the fisher kernel for large-scale image classification. In *Computer Vision–ECCV 2010: 11th European Conference on Computer Vision, Heraklion, Crete, Greece, September 5–11, 2010, Proceedings, Part IV 11*, pages 143–156. Springer, 2010.
 17. Hanwen Xu, Naoto Usuyama, Jaspreet Bagga, Sheng Zhang, Rajesh Rao, Tristan Naumann, Cliff Wong, Zelalem Gero, Javier González, Yu Gu, et al. A whole-slide foundation model for digital pathology from real-world data. *Nature*, 630(8015):181–188, 2024.
 18. George Shaikovski, Adam Casson, Kristen Severson, Eric Zimmermann, Yi Kan Wang, Jeremy D Kunz, Juan A Retamero, Gerard Oakley, David Klimstra, Christopher Kanan, et al. Prism: A multi-modal generative foundation model for slide-level histopathology. *arXiv preprint arXiv:2405.10254*, 2024.
 19. Xiyue Wang, Junhan Zhao, Eliana Marostica, Wei Yuan, Jietian Jin, Jiayu Zhang, Ruijiang Li, Hongping Tang, Kanran Wang, Yu Li, et al. A pathology foundation model for cancer diagnosis and prognosis prediction. *Nature*, 634(8035):970–978, 2024.
 20. Anurag Vaidya, Andrew Zhang, Guillaume Jaume, Andrew H Song, Tong Ding, Sophia J Wagner, Ming Y Lu, Paul Doucet, Harry Robertson, Cristina Almagro-Perez, et al. Molecular-driven foundation model for oncologic pathology. *arXiv preprint arXiv:2501.16652*, 2025.
 21. Saghir Alfasly, Ghazal Alabtah, Sobhan Hemati, Krishna Rani Kalari, Joaquin J Garcia, and HR Tizhoosh. Validation of histopathology foundation models through whole slide image retrieval. *Scientific Reports*, 15(1):3990, 2025.
 22. Edwin D de Jong, Eric Marcus, and Jonas Teuwen. Current pathology foundation models are unrobust to medical center differences. *arXiv preprint arXiv:2501.18055*, 2025.
 23. Matouš Elphick, Samra Turajlic, and Guang Yang. Are the latent representations of foundation models for pathology invariant to rotation? *arXiv preprint arXiv:2412.11938*, 2024.
 24. Nita Mulliqi, Anders Blilie, Xiaoyi Ji, Kelvin Szolnoky, Henrik Olsson, Sol Erika Boman, Matteo Titus, Geraldine Martinez Gonzalez, Julia Anna Mielcarz, Masi Valkonen, et al. Foundation models—a panacea for artificial intelligence in pathology? *arXiv preprint arXiv:2502.21264*, 2025.
 25. Gao Huang, Zhuang Liu, Laurens Van Der Maaten, and Kilian Q Weinberger. Densely connected convolutional networks. In *Proceedings of the IEEE conference on computer vision and pattern recognition*, pages 4700–4708, 2017.

26. Hamid Reza Tizhoosh and Liron Pantanowitz. Artificial intelligence and digital pathology: challenges and opportunities. *Journal of pathology informatics*, 9, 2018.
27. Andrew Janowczyk and Anant Madabhushi. Deep learning for digital pathology image analysis: A comprehensive tutorial with selected use cases. *Journal of pathology informatics*, 7, 2016.
28. Jorge Sánchez, Florent Perronnin, Thomas Mensink, and Jakob Verbeek. Image classification with the fisher vector: Theory and practice. *International journal of computer vision*, 105(3):222–245, 2013.